International Journal of Heat and Mass Transfer 163 (2020) 120378

Contents lists available at ScienceDirect

International Journal of Heat and Mass Transfer

journal homepage: www.elsevier.com/locate/hmt

Turbulent heat transfer enhancement in the mini-channel by enhancing the original flow pattern with v-ribs

Hui Xiao, Zhichun Liu, Wei Liu*

School of Energy and Power Engineering, Huazhong University of Science and Technology, Wuhan 430074, P.R. China

ARTICLE INFO

Article history:
Received 27 April 2020
Revised 19 July 2020
Accepted 20 August 2020

Keywords:
Mini-channel heat sinks
V-ribs roughness
Thermal hydraulic performance
Longitudinal swirls flow
Turbulent flow

ABSTRACT

Turbulent heat transfer attracts continuous attention from researchers due to the high convective heat transfer performance. In the mini-channel heat sink, turbulent heat transfer enhancement measures may improve the heat transfer coefficient further and reduce the mass flow rate. However, there is lack of turbulent heat transfer enhancement researches in the mini-channel heat sink due to the difficulty caused by entrance effect. In this paper, a novel heat transfer enhancement concept of enhancing the original flow pattern was successfully applied to enhance the turbulent heat transfer in the mini-channel heat sink. The investigation was carried out in a mini-channel heat sink whose substrate size was 50mm × 50mm with Reynolds number ranging from 3600 to 6800. The original flow pattern in the conventional heat sink was revealed firstly. Subsequently, the v-ribs roughness was applied to generate multi-longitudinal swirls flow so as to enhance the original flow pattern. The numerical results indicated that the variation ranges of Nu/Nu_0, f/f_0, EEC, and R3 were 1.71–3.55, 2.76–7.99, 0.32–0.89, and 1.12–2.06, respectively, in the mini-channel. Besides, the maximum average heat flux of the substrate could achieve 5.79 W/mm^2 within a temperature difference of 60 K. In addition, this paper also investigated the thermal resistance and irreversibility in the mini-channel heat sink. This work may promote the development of heat transfer enhancement.

1. Introduction

Mini/micro-channel is widely applied in electronic industry, electrical vehicles, solar cells, nuclear industry, and etc. [1]. Mini/micro-channel can be used to construct high efficient compact heat exchangers, heat sinks, and heat regenerators. In 1981, Tuckerman and Pease firstly introduced the mini/micro channel heat sink [2]. Since then, mini/micro-channel has played a significant role in the field of electronic cooling. The turbulent flow in mini-channel heat sinks can bring in high heat flux dissipation and uniform substrate temperature [3]. However, the increase in Reynolds number may cause high pump power consumption, large circulation flow rate, as well as high flow noise. Therefore, the turbulent heat transfer in mini-channel heat sinks should be enhanced so as to achieve high heat flux dissipation with moderate flow resistance penalty and circulation flow rate.

In the mini-channel heat sink, the entrance effect is significant due to the limitation of channel length. The inlet velocity and temperature distributions are approximately uniform. Due to the large viscous resistance near the channel wall, the fluid flows from the boundary region to the core flow region, thereby generating secondary flows when flowing forward. By means of generating secondary flows, efficient convective heat transfer is achieved in the mini-channel heat sinks. However, when the fluid flows forward in the mini-channel, the intensity of original secondary flows is decreased gradually, thereby deteriorating the heat transfer performance.

There are two available aspects for enhancing single phase convective heat transfer coefficient [4,5]. On the one hand, the velocity field could be altered to deflect the working fluid from the low temperature gradient region to the high temperature gradient region as well as increase the synergy between velocity field and temperature field. On the other hand, the temperature field could be altered to form a temperature distribution of alternate warm fluid and cold fluid as well as decrease the mean temperature difference between wall and working fluid.

In order to enhance the turbulent heat transfer with moderate pressure drop penalty, researchers focused attentions on the heat transfer enhancement techniques near the heat transfer surface, such as corrugations, winglets, grooves, ribs, and etc. [6]. Liu et al. [7] numerically investigated the effect of spirally corrugated tubes on shell side thermal hydraulic performance in the rod-baffle heat exchanger with Reynolds number ranging from 6000 to 18,000.

* Corresponding author.
E-mail address: w_liu@hust.edu.cn (W. Liu).

https://doi.org/10.1016/j.ijheatmasstransfer.2020.120378
0017-9310/

Nomenclature

A_b	substrate area
A_c	conjugate interface area
c_p	specific heat capacity
D_h	hydraulic diameter
e	rib height
e/W_c	height ratio
EEC	efficiency evaluation criterion
E_{xd}	exergy destruction
f	friction factor
G_d	entransy dissipation
h	heat transfer coefficient
H	heat sink height
H_c	mini-channel height
H_d	heat consumption
I	disturbance intensity
k	turbulence kinetic energy
L	heat sink length
L_1	outlet length in simulations
Lu	local heat convection number
Nu	Nusselt number
p	pressure
p_i	inlet rib pitch
p_l	longitudinal rib pitch
p_l/D_h	longitudinal pitch ratio
Pr	Prandtl number
q	substrate heat flux
R	thermal resistance
R3	overall performance criterion
Re	Reynolds number
S_g	entropy generation
T	temperature
T_0	ambient temperature
T_b	substrate temperature
T_{in}	inlet fluid temperature
T_m	mean fluid temperature
T_w	conjugate interface temperature
$u_{yz,m}$	tangential mean velocity
u_m	inlet mean velocity
u,v,w	velocity components
V_h	heat convection velocity
W	heat sink width
W_b	simplified unit width
W_c	mini-channel width
x,y,z	Cartesian coordinates

Greek symbols

α	inclined angle of ribs
β	synergy angle
κ_{eff}	effective thermal conductivity
κ_f	fluid thermal conductivity
κ_s	solid thermal conductivity
μ	dynamic viscosity
μ_t	turbulent viscosity
μ_{eff}	effective dynamic viscosity
ρ	fluid density
Φ	viscous heat dissipation
ω	specific dissipation rate

The overall performance factor of 1.35 was achieved with the one-start spirally corrugated tubes. Sun et al. [8] experimentally investigated the effect of rectangular winglet vortex generators on the turbulent thermal-hydraulic performance in circular heat exchanger tubes for $5500 \leq Re \leq 20,000$. The maximum enhancement in Nusselt number and friction factor were 2.32 and 11.63 times, respectively. Liu et al. [9] proposed novel cylindrical grooves in rectangular channels and determined the optimal configurations for turbulent heat transfer numerically. Li et al. [10] experimentally and numerically investigated the heat transfer and flow characteristics in the discrete double inclined ribs tube with Reynolds number ranging from 15,000 to 60,000. The longitudinal vortex was observed and the maximum enhancement in Nusselt number and friction factor was 1.2 and 2.5 times compared with the plain tube. Ma et al. [11] numerically studied the effect of physical properties and rib heights on thermal hydraulic performance in the high temperature channel in turbulent flow. Singh et al. [12] experimentally investigated the heat transfer and friction factor for solar air heaters with arc-shaped ribs. When Reynolds number ranging from 2200 to 22,000, the maximum enhancement in Nusselt number and friction factor were 5.07 and 3.71 times compared with the smooth solar air heater. Promvonge and Skullong [13] experimentally investigated the thermal performance of solar receivers with combined punched-V-ribs and chamfer-V-grooves with Reynolds number between 5300 and 23,000. The maximum thermal performance factor was around 2.47 where Nusselt number and friction factor were increased by 6.52 and 38.67 times over the smooth duct. Other typical turbulent heat transfer enhancement works can be found in the literature [14-16]. There are also a few research works in the field of turbulent heat transfer enhancement in mini-channel heat sinks. Dai et al. [17] collected an experimental database from the literature and investigated the friction factor in the roughened mini-channel. When the relative roughness is less than 1%, the roughness had little effect on friction factor compared with the smooth duct. Bi et al. [18] proposed an enhanced mini-channel heat sink with cylindrical grooves and dimples. For a Reynolds number range of 2700–6100, the numerically results showed that the Nusselt number could be enhanced to 2.2 times. Attalla et al. [19] experimentally investigated the effect of roughness on the heat transfer and flow characteristics in the rectangular mini-channel with Reynolds number varied from 1500 to 5000. The average Nusselt number was increased approximately by 122% in turbulent flow with air as working fluid. These fruitful works indicate that good results can be obtained by applying turbulent heat transfer enhancement techniques near the heat transfer surface.

Besides, in order to explore the optimal flow pattern for turbulent heat transfer, some researchers made efforts in the area of heat transfer optimization. Guo et al. [20] constructed the optimal flow pattern of the circular tube in turbulent flow based on entropy generation minimization. Chen et al. [21] carried out a comprehensive review on entropy and entransy in convective heat transfer optimization. Liu et al. [22] proposed the exergy minimization principle for heat transfer optimization. Xiao et al. [23] optimized the turbulent heat transfer in rectangular channels based on the exergy destruction minimization principle. All of the above heat transfer optimization results indicated that the multi longitudinal swirls flow was an optimized flow pattern. Furthermore, He and Tao [24] demonstrated that the multi longitudinal swirls flow could improve the synergy effect between temperature field and velocity field. Liu et al. [25] demonstrated that the multi longitudinal swirls flow was conducive to convective heat and mass transfer enhancement through multi-field synergy analysis. In addition, Zheng et al. [26] reviewed lots of heat transfer enhancement structures which formed multi- longitudinal swirls flow. These structures were always efficient. Therefore, the multi-longitudinal swirls flow is a good choice for heat transfer enhancement in turbulent flow.

These above reviews indicate that turbulent heat transfer enhancement is a hot and meaningful topic. However, the research works are not enough in the field of turbulent heat transfer

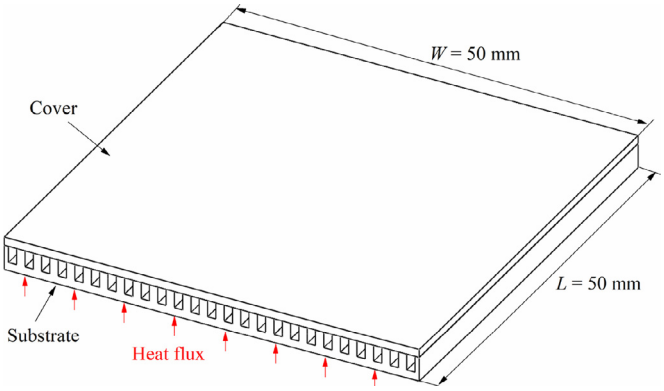

Fig. 1. The whole schematic of the selected mini-channel heat sink.

enhancement in mini-channel heat sinks. Particularly, there is scarcely any research of turbulent heat transfer enhancement focusing on the entrance region of mini-channel heat sinks. It can be attributed to the difficulty of turbulent heat transfer enhancement in mini-channels. On the one hand, it is hard to enhance the convective heat transfer due to the entrance effect. On the other hand, the flow resistance may be increased significantly with common heat transfer enhancement treatments. Thus, it motivates the authors to explore suitable heat transfer enhancement measures for the turbulent heat transfer in mini-channels.

A novel idea strikes the authors. The thermal hydraulic performance may be improved significantly by forming the multi-longitudinal swirls flow to enhance the original secondary flow in the mini-channel. In order to implement this idea, the v-rib roughness is proposed for the mini-channel. In the following text, this paper will display the original flow pattern in the conventional mini-channel heat sink firstly. Subsequently, the v-ribs will be used to periodically enhance the original flow pattern and the convective heat transfer mechanism will be revealed. Furthermore, this paper will evaluate the overall performance in the v-ribs roughened mini-channel. In the end, some conclusions will be drawn.

2. Mini-channel heat sinks

2.1. Conventional mini-channel

As depicted in Fig. 1, the selected conventional mini-channel heat sink consists of a substrate, a cover, and 25 smooth mini-channels. The dimension of the substrate is 50 mm × 50 mm, which is similar to that in the literature [3]. The heat flux is imposed on the substrate and transferred to the working fluid in the mini-channels. Subsequently, the transferred heat is taken away as the working fluid flows through the mini-channels. In the present paper, a single mini-channel is picked to investigate the thermal hydraulic performance for simplicity, as depicted in Fig. 2. Both of the left and right sides are symmetry. The heat flux is imposed on the bottom and the top is adiabatic. The total length is 55 mm, which consists of a test section of 50 mm and an outlet section of 5 mm. The height (H) and width (W_b) of the simplified model are 3 mm and 2 mm, respectively. The height (H_c) and width (W_c) of the mini-channel are 2 mm and 1 mm, respectively. Thus, the hydraulic diameter (D_h) is 1.33 mm.

2.2. V-ribs roughened mini-channel

In order to enhance the turbulent heat transfer in the mini-channel heat sink, the v-rib roughness is applied to the conventional mini-channel, as depicted in Fig. 3. The distance (p_i) between the first v-rib and the inlet is 1 mm. The v-rib height ratio (e/W_c) is 0.1. The inclined angle (α) of the v-rib is 30°, 45°, and 60°, respectively. And the longitudinal pitch ratio (p_l/D_h) is 1, 2, and 3, respectively. Other parameters are all the same as those of the conventional mini-channel.

3. Research methods

3.1. Governing equations

The present steady conjugate heat transfer problem contains a fluid domain and a solid domain. Water is chosen as the working fluid for the fluid domain and copper is selected to construct the solid substrate. The energy equation for the solid domain is written as:

$$\frac{\partial}{\partial x_i}\left(\kappa_s \frac{\partial T}{\partial x_i}\right) = 0 \tag{1}$$

where $\kappa_s = 387.6\ \mathrm{W/(m \cdot K)}$.

As for the three dimensional turbulent flow in the fluid domain, the Reynolds-averaged Navier-Stokes equations are employed. The working fluid water is considered continuum and incompressible [3]. Besides, the effect of gravity and radiation are both neglected. Compared with the transferred high heat flux, the viscous dissipation of the energy equation is also negligible. Thus, the governing equations can be written as follows:

Continuity equation:

$$\frac{\partial(\rho u_i)}{\partial x_i} = 0 \tag{2}$$

Momentum equation:

$$\frac{\partial}{\partial x_j}\left(\rho u_i u_j\right) = -\frac{\partial p}{\partial x_i} + \frac{\partial}{\partial x_j}\left[\mu_{\mathrm{eff}}\left(\frac{\partial u_i}{\partial x_j} + \frac{\partial u_j}{\partial x_i}\right)\right] \tag{3}$$

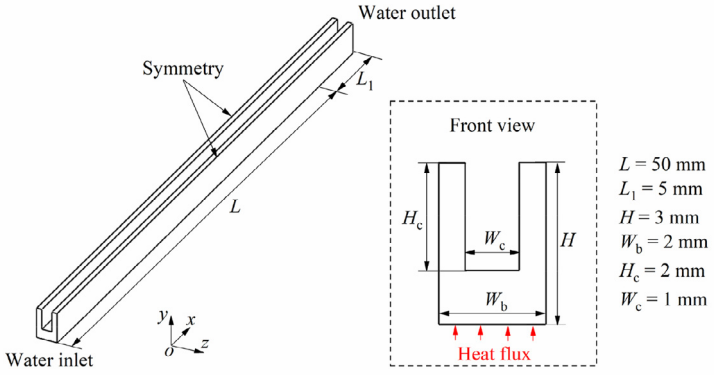

Fig. 2. The simplified conventional mini-channel for research.

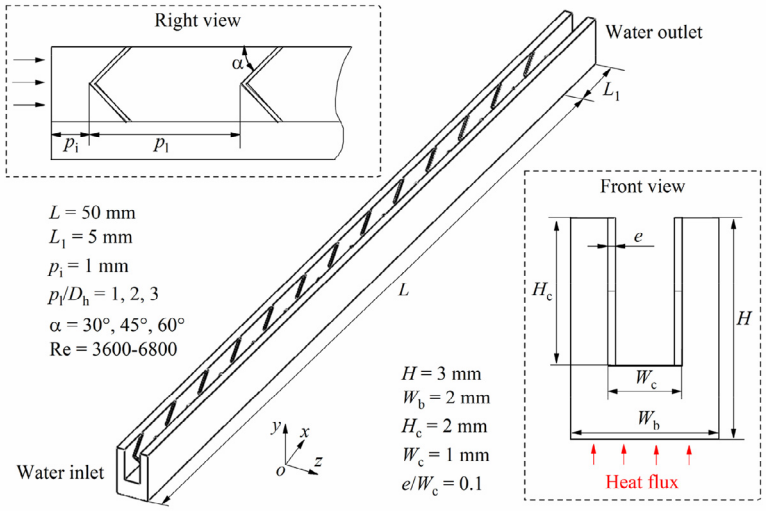

Fig. 3. The v-ribs roughened mini-channel for research.

Table 1
The variation of dynamic viscosity with temperature.

T /K	μ /10^{-6}Pa · S	T /K	μ /10^{-6}Pa · S	T /K	μ /10^{-6}Pa · S
283.15	1305.9	313.15	652.7	343.15	403.6
293.15	1001.6	323.15	546.5	353.15	354.1
303.15	797.2	333.15	466.0	363.15	314.2

Energy equation:

$$\frac{\partial}{\partial x_i}(\rho u_i c_p T) = \frac{\partial}{\partial x_i}\left(\kappa_{\text{eff}}\frac{\partial T}{\partial x_i}\right) + \Phi \tag{4}$$

where $\rho = 998.2$ kg/m^3, $c_p = 4182$ J/(kg · K), $\mu_{\text{eff}} = \mu + \mu_t$, $\kappa_{\text{eff}} = \kappa_f + \mu_t/Pr_t$, $\kappa_f = 0.6$ W/(m · K), $Pr_t = 0.85$, μ satisfies the piecewise linear function of temperature as shown in Table 1 [27], and μ_t is evaluated by the turbulence model.

The turbulence is handled by the SST k–ω turbulence model [28], which is recommended in literatures [29]. Thus, the μ_t cam be evaluated with k and ω. This turbulence model is expressed as:

$$\frac{\partial}{\partial x_i}(\rho k u_i) = \frac{\partial}{\partial x_i}\left(\Gamma_k\frac{\partial k}{\partial x_i}\right) + G_k - Y_k \tag{5}$$

$$\frac{\partial}{\partial x_i}(\rho \omega u_i) = \frac{\partial}{\partial x_i}\left(\Gamma_\omega\frac{\partial \omega}{\partial x_i}\right) + G_\omega - Y_\omega \tag{6}$$

3.2. Boundary conditions

At the inlet of the fluid domain, a uniform velocity distribution is specified with a constant turbulence intensity of 5% when Reynolds number ranging from 3600 to 6800. The inlet temperature is uniform at 293.15 K. At the outlet of the fluid domain, the pressure outlet is specified. At the interface between fluid domain and solid domain, the coupled boundary is specified for the energy equation and the no slip boundary is specified for the momentum equation. At the top of the mini-channel heat sink, the no slip boundary is specified for the fluid domain and the adiabatic thermal boundary condition is imposed on both of the fluid domain and solid domain. As for the left and right sides of the solid domain, the symmetry boundary is specified. At the bottom of the solid domain, a uniform heat flux of 1 W/mm^2 is imposed for investigating the thermal hydraulic performance, while a uniform temperature of 353.15 K is imposed for investigating the maximum supportable heat flux.

3.3. Parameter definitions

In order to characterize the turbulent heat transfer in the mini-channel heat sink, some parameters are introduced and defined in the following.

Hydraulic diameter:

$$D_h = \frac{2W_cH_c}{W_c + H_c} \tag{7}$$

Reynolds number:

$$\text{Re} = \frac{\rho u_m D_h}{\mu} \tag{8}$$

where u_m is the mean velocity at the inlet of the fluid domain.

Friction factor:

$$f = \frac{\Delta p}{(L/D_h)\rho u_m^2/2} \tag{9}$$

where Δp is the pressure difference in the test section.

The equivalent convective heat transfer coefficient (h) is used to involve in the effect of increased heat transfer area. It is defined as:

$$h = \frac{qA_b}{A_c(T_w - T_m)} \tag{10}$$

where q is the heat flux at the bottom of the substrate, T_w is the average temperature of the conjugate fluid-solid interface, T_m is the mean temperature of the working fluid, and A_b and A_c are the area of the substrate and fluid-solid interface in the conventional mini-channel, respectively.

Nusselt number:

$$Nu = \frac{hD_h}{\kappa_f} \tag{11}$$

The disturbance intensity is defined as:

$$I = u_{yz,m}/u_m \tag{12}$$

where $u_{yz,\,m}$ is the mass weighted average tangential velocity perpendicular to the flow direction.

The thermal resistance can be defined as:

$$R_{tot} = \frac{T_{b,\max} - T_{in}}{qA_b},\ R_{sol} = \frac{T_{b,\max} - T_w}{qA_b},\ R_{flu} = \frac{T_w - T_{in}}{qA_b} \tag{13}$$

where R_{tot}, R_{flu}, and R_{sol} are total thermal resistance, fluid thermal resistance, and substrate thermal resistance, respectively.

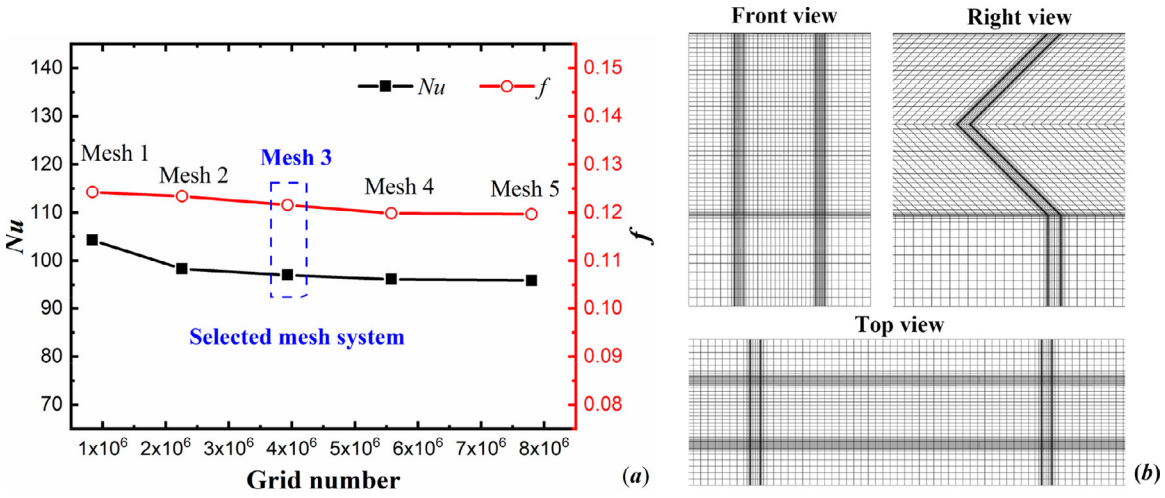

Fig. 4. (*a*) Grid independence verification and (*b*) grid system details.

In order to evaluate the overall thermal hydraulic performance, the criterion R3 [30] is adopted and defined as:

$$\mathrm{R3} = Nu/Nu_c \tag{14}$$

where Nu_c is the equivalent Nusselt number in the smooth mini-channel at an identical pump power consumption. In detail, Nu_c is the Nusselt number of the smooth mini-channel at the equivalent Reynolds number Re_c. The Re_c can be calculated with

$$f_c \mathrm{Re}_c{}^3 = f\mathrm{Re}^3 \tag{15}$$

Besides, the criterion EEC is selected as an auxiliary criterion so as to evaluate the performance at an identical mass flow rate. It is defined as:

$$\mathrm{EEC} = \frac{Nu/Nu_0}{f/f_0} \tag{16}$$

where Nu_0 and f_0 are Nusselt number and friction factor of the smooth mini-channel at the Reynolds number *Re*, respectively. The *Re* is identical to that in the enhanced mini-channel.

3.4. Computational methods

The numerical research is carried out with the commercial software FLUENT 16.0. The computational domain is covered by a structural mesh generated by the commercial software ICEM 16.0. The mesh is extremely dense near the fluid-solid interface, which guarantees $y^+ < 1$. The governing equations are discretized with finite volume method. The second order discretization is applied for pressure while the second order upwind scheme is used to handle the nonlinear convection-diffusion problem for momentum, energy, and turbulence equations. The SIMPLE algorithm is employed to deal with the coupling of pressure and velocity [31-33]. The SST k–ω turbulence model is activated to deal with the turbulence. When the relative residuals are less than 10^{-4} for continuity equation, 10^{-8} for energy equation, and 10^{-6} for other equations, or all relative residuals keep constant, the results can be considered converged and reliable.

3.5. Results verifications

The grid independence verification is carried out firstly. Five mesh systems are generated from coarse to dense as: Mesh1 (0.84 million), Mesh2 (2.26 million), Mesh3 (3.93 million), Mesh4 (5.58 million), and Mesh5 (7.80 million). The grid independence verification results are obtained in the v-ribs roughened mini-channel with $\alpha = 45^\circ$, $p_l/D_h = 3$, and $Re = 5200$. As depicted in Fig. 4(*a*), when the grid number increases from 3.93 million to 7.80 million, the discrepancy of Nusselt number and friction factor are 1.2% and 1.6%, respectively. It indicates that the grid system of Mesh3 is dense enough to capture the present turbulent flow. Besides, the mesh details of Mesh3 are displayed in Fig. 4(*b*). It can be seen that the structural mesh is dense and well-shaped, which helps to obtain accurate results. Thus, the grid system of Mesh3 is selected for the following research.

The accuracy of the numerical results are verified by comparing with the empirical formulas in the smooth duct. The empirical formulas are suggested in Refs. [18,30,34]. For Nusselt number, the Gnielinski equation is expressed as:

$$Nu_0 = \frac{(f/8)(\mathrm{Re} - 1000)\,\mathrm{Pr}}{1 + 12.7\sqrt{f/8}\left(\mathrm{Pr}^{2/3} - 1\right)} \cdot M \tag{17}$$

where f is the friction factor in the fully developed smooth duct and the multiplier M represents the correction to the Nusselt number with considering the combined effect of entrance and temperature difference between fluid and wall.

The friction factor can be predicted by Filonenko equation as:

$$f_0 = f \cdot M \tag{18}$$

$$f = (1.82 \lg \mathrm{Re} - 1.64)^{-2} \tag{19}$$

The multiplier M is also available for correcting friction factor in Eq. (18) when considering the entrance effect and temperature difference between fluid and wall. The multiplier M is expressed as

$$M = \left[1 + (D_h/L)^{2/3}\right](\mathrm{Pr}/\mathrm{Pr}_w)^c \tag{20}$$

where c is 0.11 and −0.25 for Nusselt number and friction factor under the heating condition, respectively.

The comparisons of Nusselt number and friction factor between numerical and empirical results are depicted in Fig. 5. The numerical results are obtained by applying five turbulence models which are RNG k-ε model, Realizable k-ε model, SST k-ω model, Transition SST model, and k-kl-ω Transition model, respectively. The numerical results obtained by SST k-ω model agree well with the empirical results. The maximum deviations in Nusselt number and friction factor are 9.1% and 3.8% compared with the empirical results, respectively. It indicates that the computational process is right and that the SST k-ω model can provide accurate results in the research range of this paper. Thus, the results in the following are reliable.

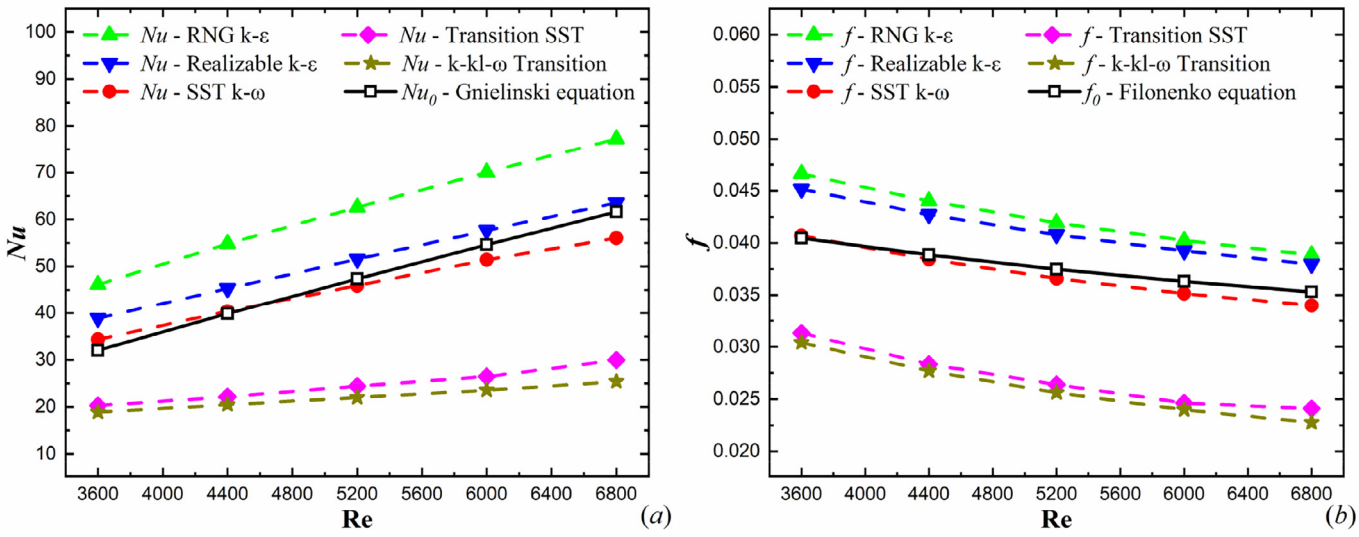

Fig. 5. Verifications with empirical formulas: (*a*) Gnielinski equation; (*b*) Filonenko equation.

4. Original flow pattern in conventional mini-channels

The original flow pattern is the flow pattern in the conventional smooth mini-channel heat sink. As for the channel flow, the flow pattern can be characterized by the tangential velocity distribution in the cross section. In terms of turbulent heat transfer in the mini-channel, the original flow pattern is caused by the velocity entrance effect. Due to the combined effect of velocity entrance and thermal entrance, the heat transfer coefficient in the entrance region is much higher than that in the fully developed region. If the heat transfer enhancement measure disrupts the original flow pattern greatly, the fluid disturbance may be useless. It leads to high power consumption with little heat transfer enhancement harvest. On the contrary, if the heat transfer enhancement measure enhances the original flow pattern, the turbulent heat transfer coefficient may be significantly enhanced with a moderate increase of pump power consumption, which leads to the improvement in thermal hydraulic performance. Thus, it is meaningful to investigate the original flow pattern in the conventional smooth mini-channel heat sink. In the following of this part, a constant heat flux of 1 W/mm^2 is specified at the bottom of the substrate.

Fig. 6 shows the tangential velocity distributions and the corresponding simplified flow patterns at five cross sections for $Re = 5200$. The cross sections are located in the fluid domain of conventional mini-channel heat sink at $x/L = 0.1$, 0.3. 0.5, 0.7, and 0.9, respectively. At the inlet, the velocity and temperature distributions are uniform. At the cross section of $x/L = 0.1$, due to the larger viscous resistance near the channel wall, the fluid flows from the boundary region to the core flow region, thereby generating secondary flows. When the fluid passes by the cross sections of $x/L = 0.3$ and 0.5, the left-right counter flow intensity is gradually decreased with the increase of mass flow rate in the core region. When fluid passes by the cross sections of $x/L = 0.7$ and 0.9, the up-down transverse counter flow, which is noted with red arrows in Fig. 6, is still there. Besides, due to the excessive viscous resistance caused by the gradually increased mass flow rate in the core flow region, the fluid in the core flow region flows to the left and right wall. In this way, the longitudinal swirls flow is generated. On the whole, the up-down counter flow is the main characteristic of the original flow pattern, and the transverse secondary flow intensity weakens gradually when flowing forward. Hence, the heat transfer enhancement measure is recommended to form the up-down counter flow so as to prevent the excessive penalty of pressure drop.

Fig. 7 shows the temperature distributions at five cross sections of $x/L = 0.1$, 0.3. 0.5, 0.7, and 0.9, respectively, in the fluid and solid domains for $Re = 5200$. With the fluid flowing forward, the velocity and thermal entrance effect weaken gradually so that the thermal boundary layer in the fluid domain becomes thicker and thicker. Correspondingly, the temperature gradient near the fluid-solid interface is decreased gradually, which leads to lower convective heat transfer performance. Consequently, it causes unwanted higher substrate temperature. It indicates that the turbulent heat transfer enhancement is necessary in the mini-channel heat sink. When heat transfer enhancement measure is adopted to enhance the original secondary flow intensity, the thermal boundary layer may be thinned by intense fluid mixing, thereby enhancing the convective heat transfer performance effectively.

In conclusion, adopting heat transfer enhancement measure to enhance the up-down counter flow may achieve high thermal performance with moderate penalty of flow resistant. In order to form the up-down counter flow, the v-ribs are applied to roughen the conventional mini-channel. The flow characteristics and heat transfer performance of the v-ribs roughened mini-channel are displayed in the following part.

5. Heat transfer enhancement with v-ribs

5.1. Heat transfer enhancement characteristics

In this part, a constant heat flux of 1 W/mm^2 is specified at the bottom of the substrate for investigating the heat transfer and flow characteristics in the v-ribs roughened mini-channel heat sink. The enhanced flow pattern and temperature distributions are investigated firstly. Subsequently, the local heat convection performance is investigated by heat convection velocity analysis. In addition, the thermal resistance is also investigated in this part.

5.1.1. Flow patterns and temperature distributions

The three dimensional streamlines in v-ribs roughened mini-channels are depicted in Fig. 8. The inclined angle (α) of the v-rib is 30°, 45°, and 60°, respectively. The longitudinal pitch ratio (p_l/D_h) is 2 and the Reynolds number is 5200. In the front view of the mini-channel, four longitudinal swirls are formed whether α

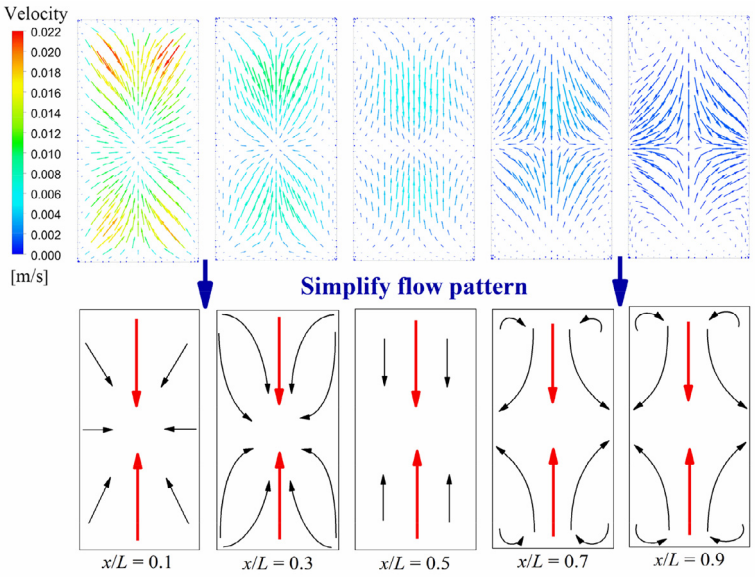

Fig. 6. Tangential velocity distributions and simplified flow patterns at x/L = 0.1, 0.3. 0.5, 0.7, and 0.9 in the conventional mini-channel.

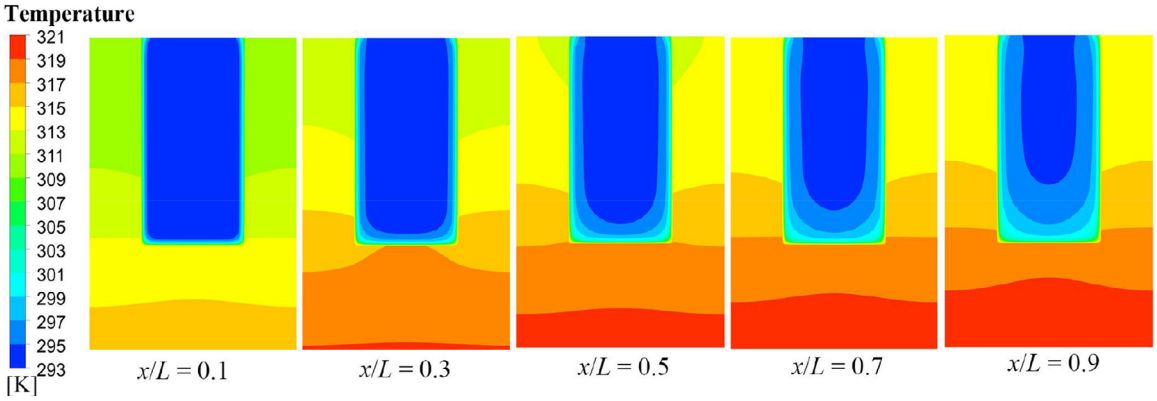

Fig. 7. Temperature distributions at x/L = 0.1, 0.3. 0.5, 0.7, and 0.9 in the conventional mini-channel.

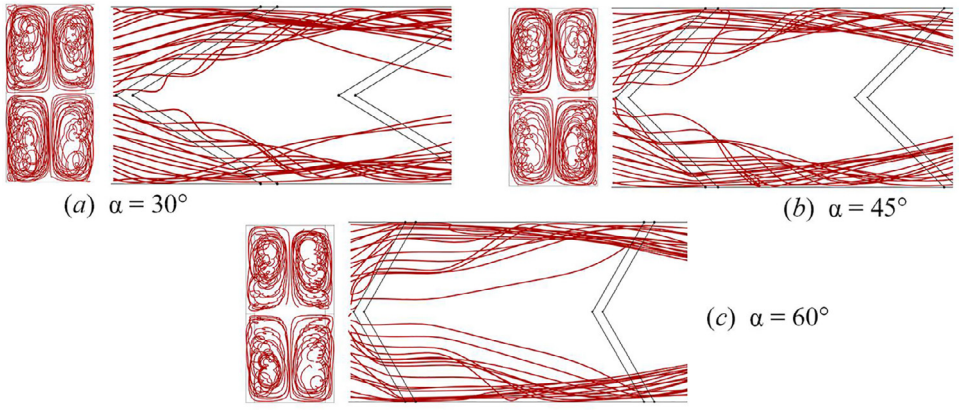

Fig. 8. Streamlines in the v-ribs roughened mini-channel with p_l/D_h = 2 and Re = 5200 for different inclined angles.

is 30°, 45°, or 60° Besides, the streamlines are affected by the inclined angle significantly. When the inclined angle increases from 30° to 45°, the streamlines become more curved. However, the streamlines bypass the v-ribs and the curvature becomes smaller when the inclined angle increases from 45° to 60° In conclusion, with applying v-ribs in the mini-channel, the fluid are disturbed significantly and the multi-longitudinal swirls flow is formed.

The tangential velocity and temperature distributions in the v-ribs roughened mini-channel are depicted in Figs. 9 and 10, respectively. The working condition is $\alpha = 45°$, $p_l/D_h = 2$, and $Re = 5200$. The tangential velocity distributions are taken from five cross sections in the fluid domain. As depicted in Fig. 9, two pairs of vortices can be seen in each cross section and the up-down counter flow is enhanced compared with the conventional mini-channel.

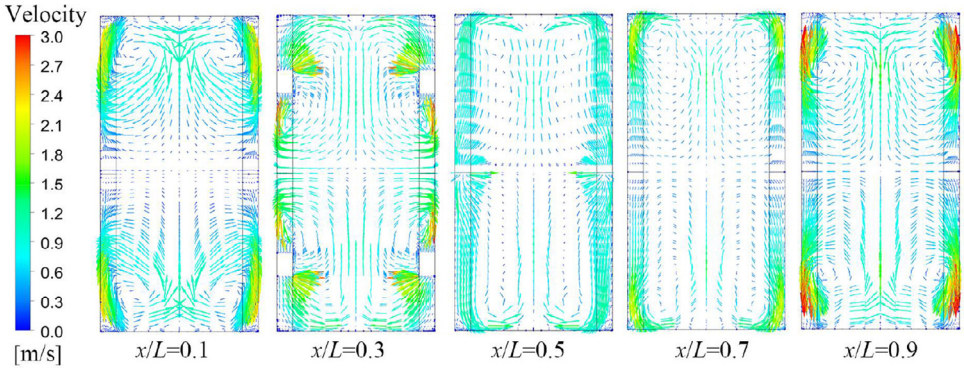

Fig. 9. Tangential velocity distributions at several cross sections in the fluid domain of the v-ribs roughened mini-channel.

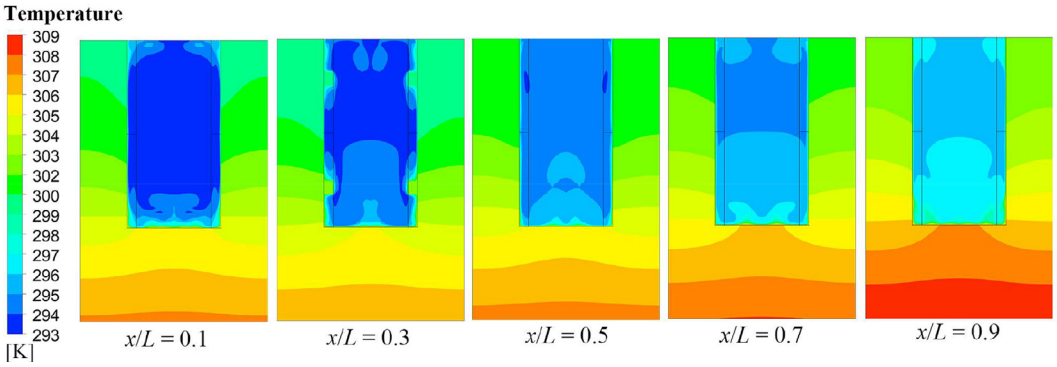

Fig. 10. Temperature distributions at several cross sections in the whole domain of the v-ribs roughened mini-channel.

Thus, the original flow pattern is successfully enhanced by roughening the mini-channel with v-ribs. The temperature distributions are taken from five cross sections in the whole domain. As depicted in Fig. 10, due to the longitudinal swirls flow, the cross section temperature in the fluid domain becomes an alternative distribution of warm and cold fluid. It is conducive to enhancing the heat transfer inside the fluid. Furthermore, the thermal boundary layer in the fluid domain is disrupted and extremely thin, which is conducive to decreasing the temperature difference between solid and fluid. Comparing Fig. 10 with Fig. 7, the temperature difference between the maximum temperature and inlet temperature is approximately decreased by 43%. In this way, the thermal performance is improved by roughening the mini-channel with v-ribs.

In order to compare the flow characteristics and heat transfer performance between the conventional and v-ribs roughened mini-channels intuitively, this paper shows the comparisons of average Nusselt number, friction factor, and disturbance intensity ($u_{yz,m}/u_m$) along the flow direction in Fig. 11. In the conventional mini-channel, the Nusselt number, friction factor, and disturbance intensity are all gradually decreased along the flow direction. In the v-ribs roughened mini-channel, the trend of these curves is different. The disturbance intensity is increased gradually due to the periodical disturbance caused by v-ribs. Though the disturbance intensity is increased, the friction factor is decreased due to the sharply decreased viscous resistance along the flow direction. Particularly, the Nusselt number decreases first and then increases. When the fluid enters the v-ribs roughened mini-channel, the thermal boundary layer thickens gradually due to insufficient disturbance intensity. Hence, the Nusselt number is decreased near the inlet. As the fluid flows forward, the fluid disturbance intensity increases gradually to enhance the convective heat transfer, thereby increasing the Nusselt number. On the whole, the Nusselt number, friction factor, and disturbance intensity in the v-ribs roughened mini-channel are larger than those in the conventional mini-channel.

5.1.2. Heat convection velocity analysis

Heat convection velocity (V_h) is the velocity component in temperature gradient direction [4]. Its magnitude is defined as

$$V_h = \frac{\mathbf{U}\cdot\nabla T}{|\nabla T|} = |\mathbf{U}|\cos\beta \tag{21}$$

where β is the included angle between velocity and temperature gradient at a local position.

The heat convection velocity can reflect the heat convection intensity at a local position. In order to describe the local heat convection performance with consideration of thermal diffusion, a new dimensionless parameter called *Lu* number is introduced as:

$$Lu = \frac{\rho c_p |V_h| D_h}{\kappa_f} \tag{22}$$

In this way, the whole convective heat transfer performance can be evaluated by *Nu* while the local heat convection performance can be evaluated by *Lu*. Increasing the *Lu*, especially in the high temperature gradient region, can lead to larger $\mathbf{U}\cdot\nabla T$, which may result in a larger *Nu*.

The *Lu* analysis is implemented in the condition of a constant substrate heat flux of 1 W/mm^2 for $Re = 5200$, so as to reveal the convective heat transfer mechanism in the mini-channel. Fig. 12 shows the comparisons of *Lu* distributions at several cross sections in the fluid domain. The results in Fig. (*a*) are taken from the conventional mini-channel which the results in Fig. (*b*) are taken from the v-ribs roughened mini-channel with $\alpha = 45^\circ$ and $p_l/D_h = 2$. As depicted in Fig. 12(*a*), at the cross section of $x/L = 0.1$, the *Lu* is relatively high in most area due to the intense secondary flow. It is the reason that the Nusselt number is high at $x/L = 0.1$ in the conventional mini-channel. As the fluid flows from $x/L = 0.5$ to

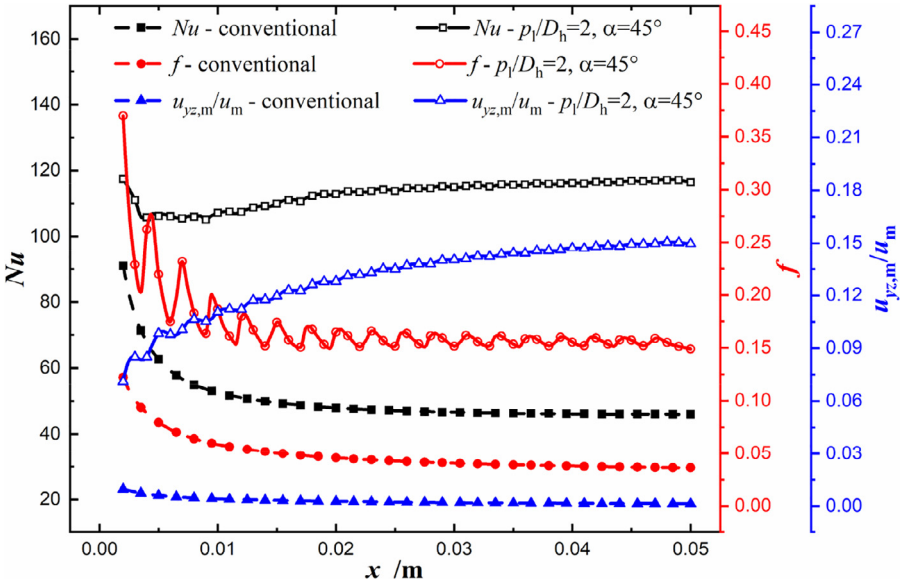

Fig. 11. Comparisons of average Nusselt number, friction factor, and disturbance intensity along the flow direction for $Re = 5200$.

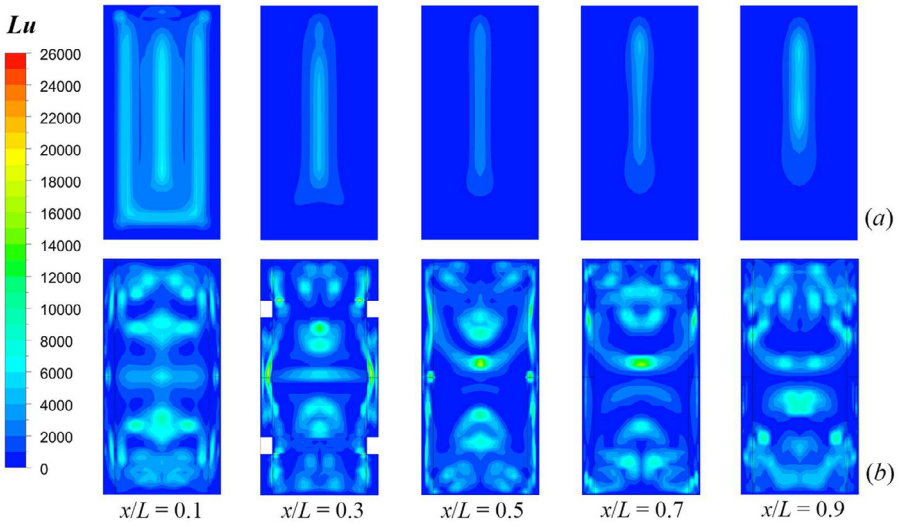

Fig. 12. Comparisons of *Lu* distributions at several cross sections in the fluid domain: (*a*) conventional mini-channel; (*b*) v-ribs roughened mini-channel.

$x/L = 0.9$, the average *Lu* is increased due to the increased left-right counter flow. Comparing Fig. 12(*b*) with Fig. (*a*), the *Lu* is increased in most area, which indicates that the local heat convection performance is increased in most area. Besides, in the region near the fluid-solid interface where the temperature gradient is high, the *Lu* is increased much. Therefore, the whole convective heat transfer performance is enhanced significantly.

5.1.3. Thermal resistance analysis

The thermal resistance analysis is carried out with a constant substrate heat flux of 1 W/mm^2. When transferring the same amount of heat, the maximum temperature difference is decreased as the thermal resistance decreases in the mini-channel heat sink. Besides, the thermal resistance analysis helps to find the dominate impediment in heat transfer process. Hence, the thermal resistance analysis is important. Fig. 13(*a*) shows the variations of average thermal resistance with the increase of inlet distance for $Re = 5200$. With the increase of inlet distance, all of the thermal resistant curves decreases as the heat transfer area increases. At the same inlet distance, both of the total thermal resistant and the fluid thermal resistant in the v-ribs roughened mini-channel heat sink are smaller than those in the conventional mini-channel heat sink, while the solid thermal resistance changes very little. As depicted in Fig. 13(*b*), with the increase of Reynolds number, both of the total thermal resistance and the fluid thermal resistance are decreased while the solid thermal resistance varies very little. Due to the enhanced convective heat transfer performance in the v-ribs roughened mini-channel, both of the fluid thermal resistance and the total thermal resistance are decreased at an identical Reynolds number. However, the solid thermal resistance in the v-ribs roughened mini-channel is slightly larger than that in the conventional mini-channel. The reason is that the enhanced convective heat transfer causes a lower and more uniform fin temperature which increases the temperature difference between the substrate and fluid-solid interface. More importantly, the fluid thermal resistance is close in value to the solid thermal resistance in the v-ribs roughened mini-channel heat sink. It indicates that fluid thermal resistance is no longer the dominate impediment of the heat transfer process. Thus, the v-ribs roughness is on the nose for enhancing the convective heat transfer performance in the mini-channel heat sink.

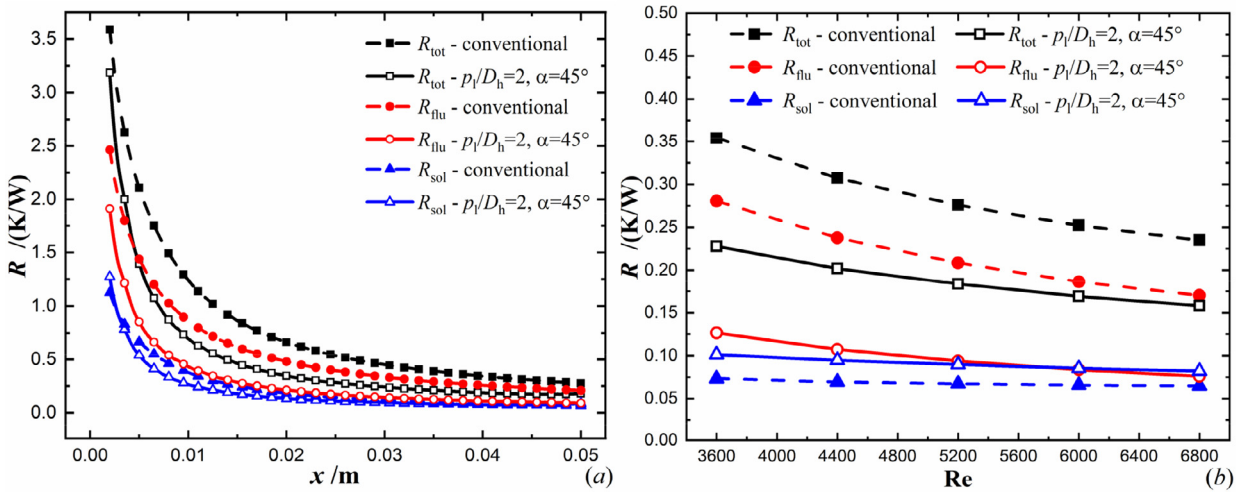

Fig. 13. Variations of average thermal resistance with the increase of (*a*) inlet distance and (*b*) *Re*.

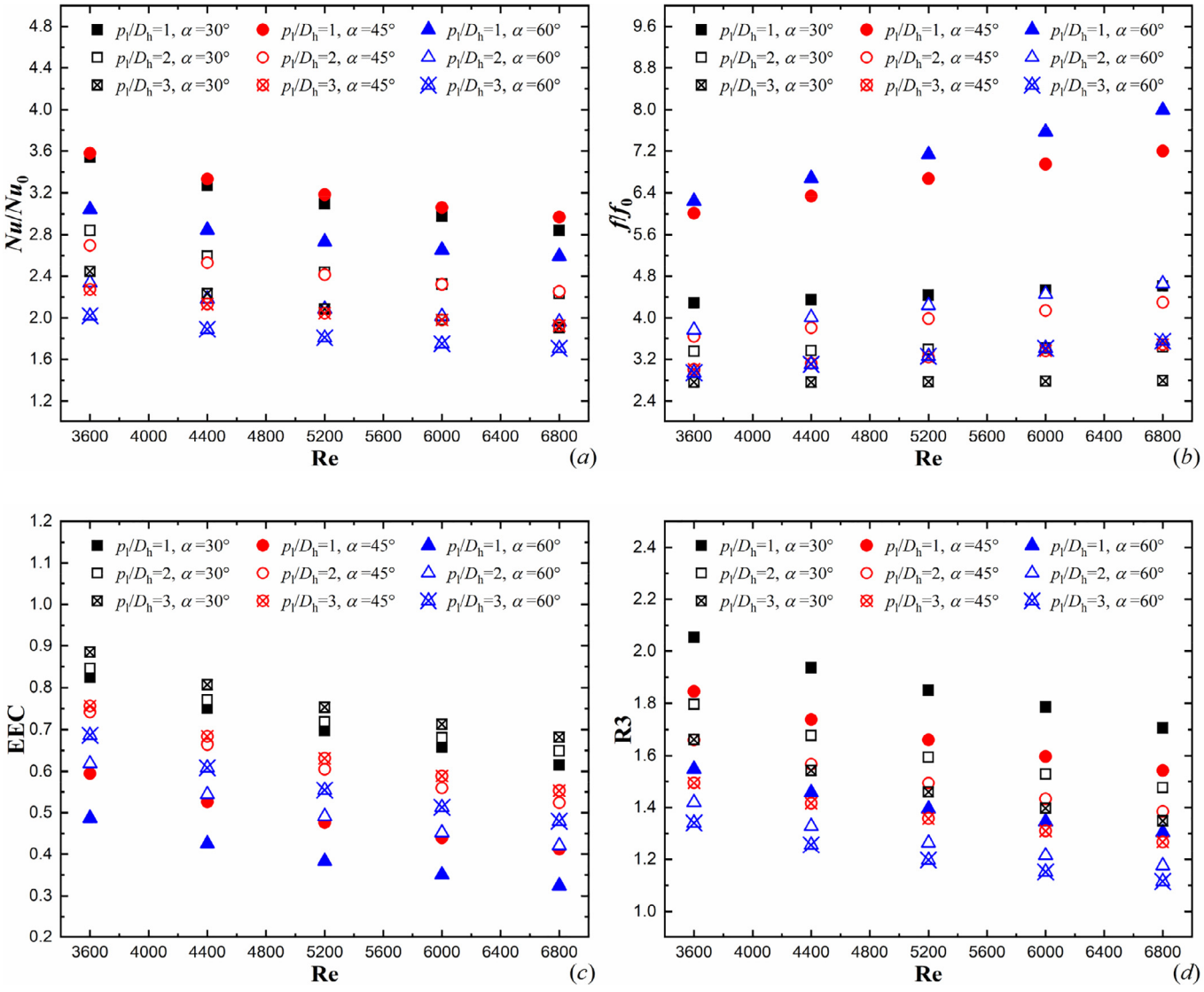

Fig. 14. Variations of Nu/Nu_0, f/f_0, EEC, and R3 with the increase of *Re*.

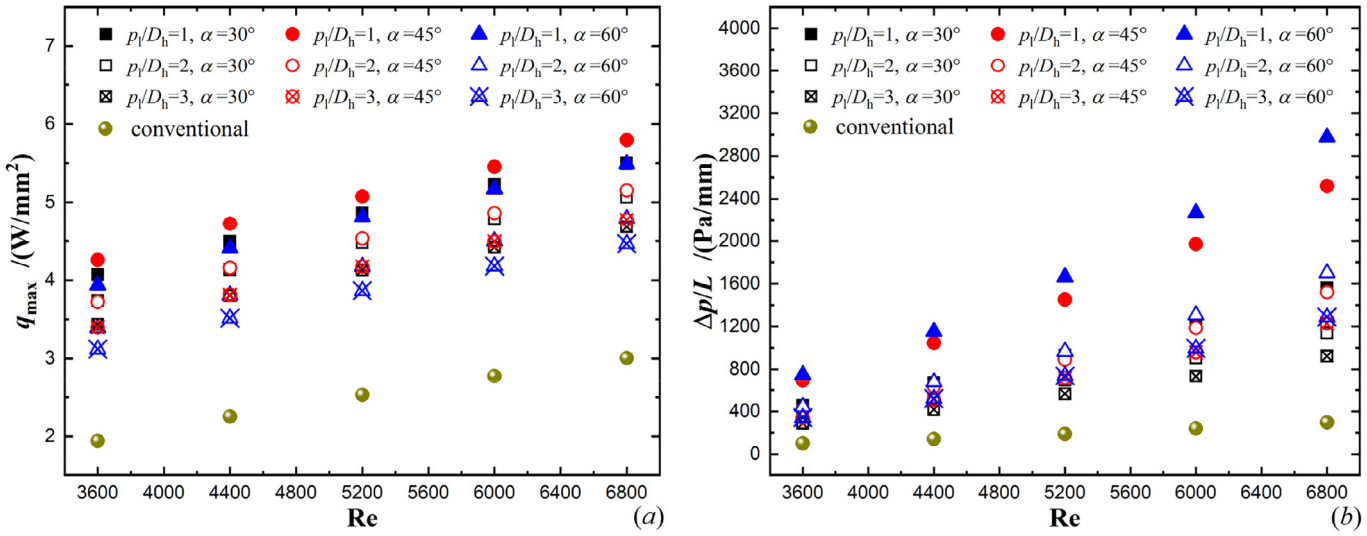

Fig. 15. Variations of average heat flux and pressure drop with the increase of *Re*.

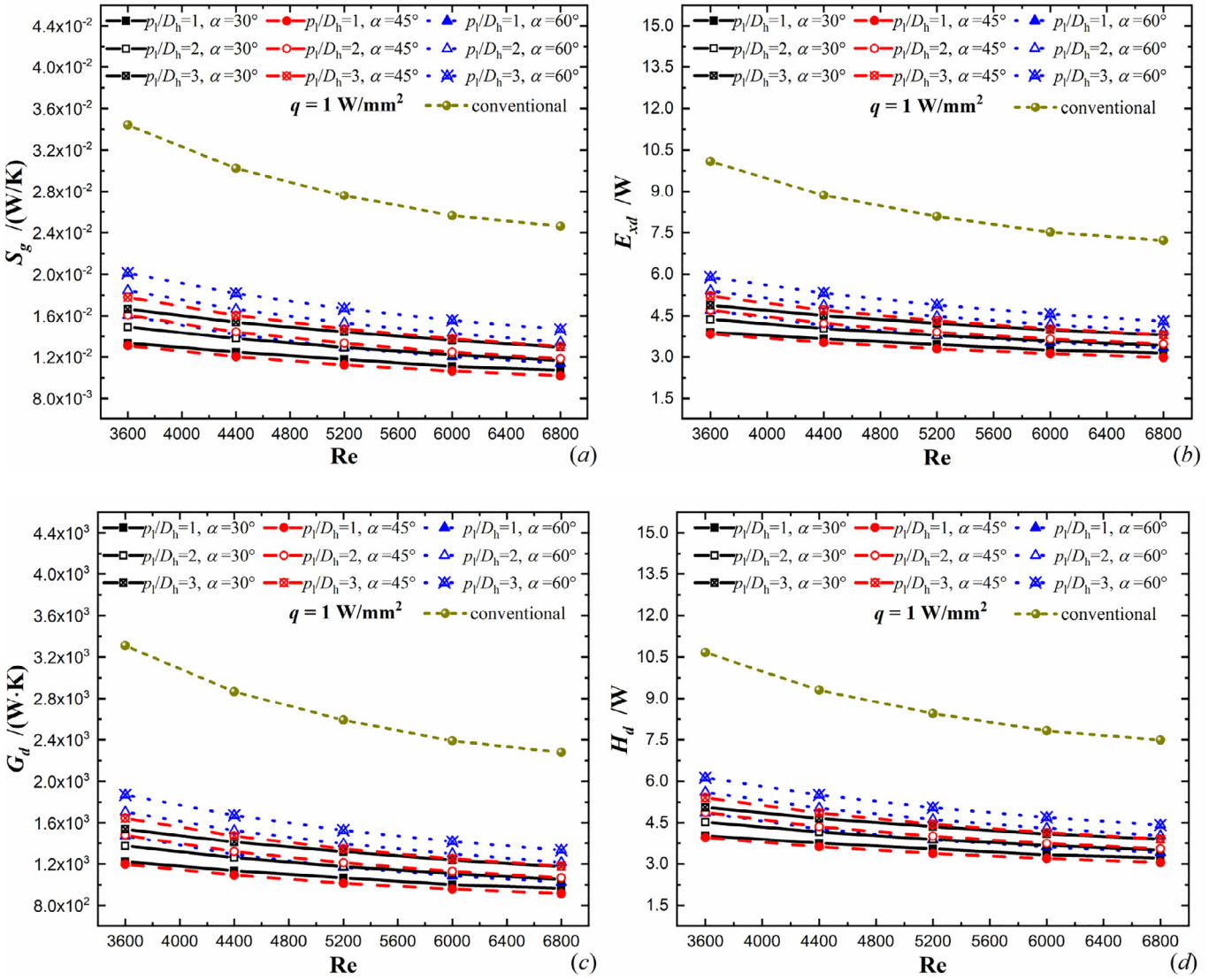

Fig. 16. Variations of S_g, E_{xd}, H_d, and G_d for q = 1 W/mm^2.

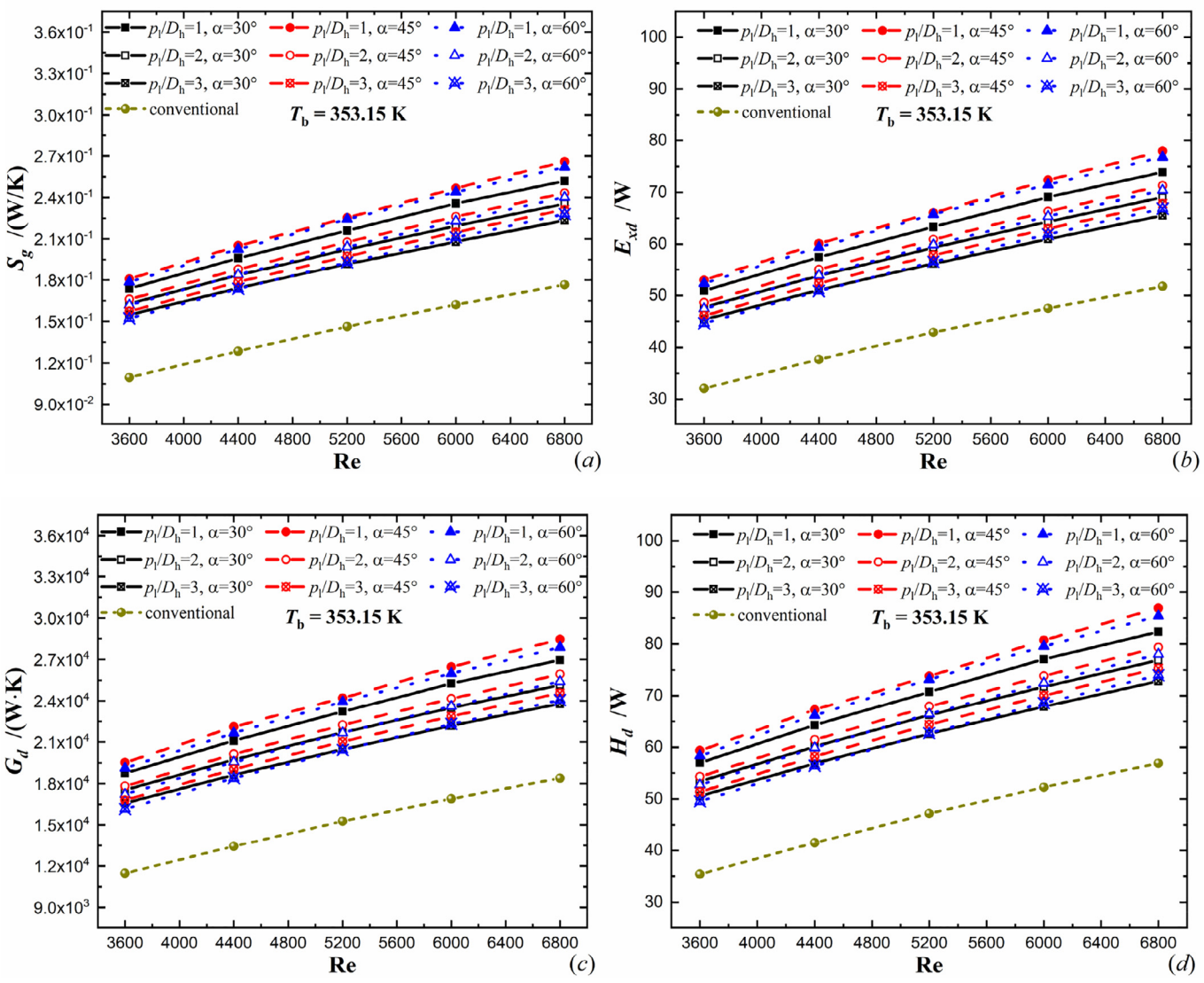

Fig. 17. Variations of S_g, E_{xd}, H_d, and G_d for T_b = 353.15 K.

5.2. Performance evaluations

5.2.1. Thermal hydraulic performance

The thermal hydraulic performance evaluation of the mini-channel is carried out with specifying a constant heat flux of 1 W/mm^2 on the substrate bottom. As depicted in Fig. 14(*a*) and (*b*), both of Nu/Nu_0 and f/f_0 are increased with the decrease of p_l/D_h. With the increase of α, the f/f_0 is increased while the variation of Nu/Nu_0 is complex. When α increases from 30° to 45°, the Nu/Nu_0 varies very little. When α increases from 45° to 60°, the Nu/Nu_0 is decreased due to the decreased effective disturbance. The variation range of Nu/Nu_0 and f/f_0 are 1.71–3.55 and 2.76–7.99, respectively. As depicted in Fig. 14(c), the variation range of EEC is 0.32–0.89. The EEC is larger than 0.5 in most cases, which indicates that the flow resistance performance is good. The overall thermal hydraulic performance is indicated by R3 criterion in Fig. 14(d). The R3 criterion is larger than 1 in all cases, which indicates that the v-ribs roughened mini-channel is always superior to the conventional mini-channel in the range of this research. The variation range of R3 is 1.12–2.06. In addition, the configured parameters of $p_l/D_h = 1$ and $\alpha = 30°$ are recommended for achieving a larger R3 criterion at an identical Reynolds number.

5.2.2. Maximum heat flux

It is meaningful to investigate the maximum heat flux that can be dissipated in the mini-channel heat sink. As depicted in Fig. 15, the average heat flux and corresponding pressure drop are obtained by specifying a constant substrate temperature of 353.15 K. In other words, the obtained average heat flux is the maximum heat flux that can be dissipated within a temperature difference of 60 K between inlet fluid temperature and substrate temperature. As shown in Fig. 15(*a*), the maximum average heat flux in the enhanced heat sink is larger than that in the conventional heat sink. The maximum average heat flux can achieve 5.79 W/mm^2 in the condition of $p_l/D_h = 1$, $\alpha = 45°$, and $Re = 6800$. The corresponding pressure gradient is 2520 Pa/mm, as depicted in Fig. 15(*b*).

5.2.3. Irreversibility analysis

Heat transfer irreversibility can be used to evaluate the heat transfer performance in the view of second law of thermodynamics. By means of reducing the heat transfer irreversibility, the available energy loss can be reduced correspondingly in the heat transfer process. It is conducive to waste heat recovery. In order to represent the heat transfer irreversibility in the mini-channel heat sink comprehensively, four typical quantities are employed as entropy generation (S_g) [35], exergy destruction (E_{xd}) [22], heat con-

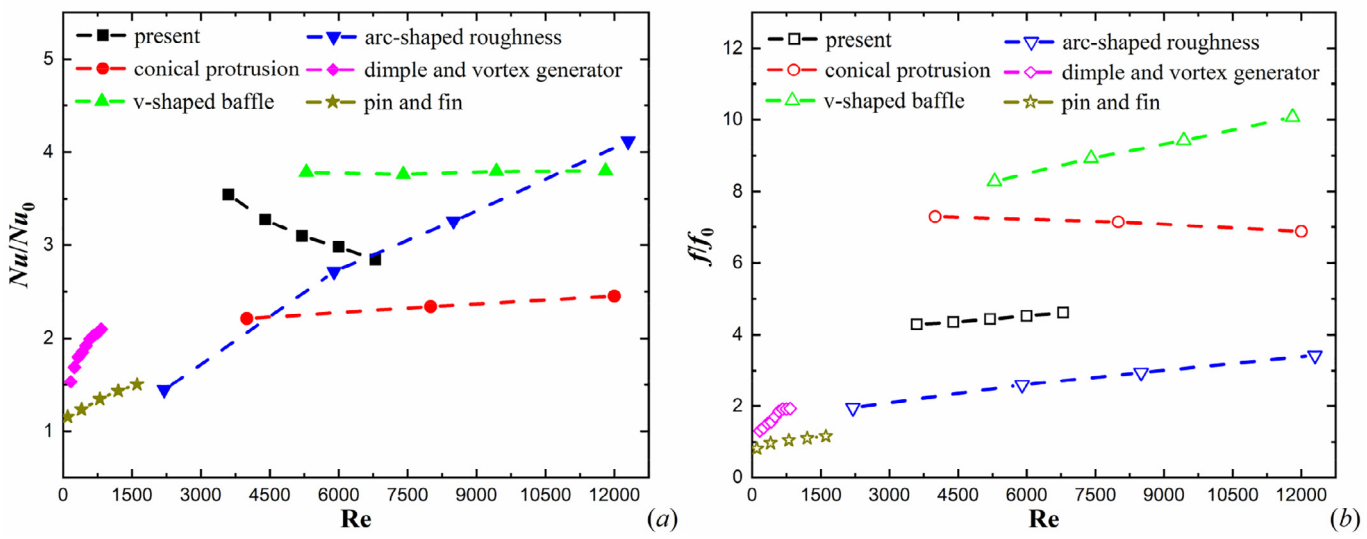

Fig. 18. Comparisons of (*a*) Nu/Nu_0 and (*b*) $\frac{Nu/Nu_0}{f/f_0}$ between present work and other published papers.

sumption (H_d) [36], and entransy dissipation (G_d) [21]. Their expressions per unit volume are given as:

$$s_g = \frac{\kappa(\nabla T)^2}{T^2},\ e_{xd} = T_0\frac{\kappa(\nabla T)^2}{T^2},\ h_d = \frac{\kappa(\nabla T)^2}{T},\ g_d = \kappa(\nabla T)^2. \tag{23}$$

where $T_0 = 293.15$ K, κ is κ_{eff} and κ_s in the fluid domain and solid domain, respectively.

The temperature gradient is validated before the following irreversibility analysis. The obtained temperature gradient is substituted into the energy equation in the fluid domain. The energy equation is satisfied. Besides, the total entropy generation that is calculated with the obtained temperature gradient also satisfies the entropy balance equation in the mini-channel heat sink. Thus, the irreversibility results calculated by the temperature gradient are all reliable.

The irreversibility values depicted in Figs. 16 and 17 are the sum of irreversibility in fluid domain and solid domain. Fig. 16 shows the variations of S_g, E_{xd}, H_d, and G_d with the increase of Reynolds number under the thermal condition of a constant heat flux on the substrate. The variation regularity of the four irreversibility indicators are similar. The S_g, E_{xd}, H_d, and G_d in the v-ribs roughened mini-channel heat sink are all smaller than those in the conventional mini-channel heat sink. The reason is that the temperature difference is decreased as the convective heat transfer is enhanced. Fig. 17 shows the variations of S_g, E_{xd}, H_d, and G_d with the increase of Reynolds number under the thermal condition of a constant substrate temperature. The variation regularity of the four irreversibility indicators are also similar. The S_g, E_{xd}, H_d, and G_d in the v-ribs roughened mini-channel heat sink are all larger than those in the conventional mini-channel heat sink. The reason is that the transferred heat flux is increased in the enhanced mini-channel heat sink.

5.3. Comparisons

The present work is aimed at enhancing the turbulent heat transfer performance in the mini-channel heat sink where the entrance effect is significant. To the authors' knowledge, there is scarcely any research of turbulent heat transfer enhancement in the entrance region of mini-channel heat sinks. In order to demonstrate the present work more comprehensively, some relevant typical heat transfer enhancement works are selected for comparison. The recommended configured parameters of $p_l/D_h = 1$ and $\alpha = 30°$ are picked out for the comparison with other previous works. The typical heat transfer components are chosen as conical protrusion [16], v-shaped baffle [20], arc-shaped roughness [12], dimple and vortex generator [37], and pin and fin [38]. As shown in Fig. 18, the enhancement times in Nusselt number is relatively high, while the increase times in friction factor is moderate. It demonstrate the effectiveness of the present work.

6. Conclusions

In this paper, the original flow pattern was investigated in the conventional smooth mini-channel heat sink where the entrance effect was significant. On this basis, the v-ribs were applied to roughen the conventional mini-channel heat sink so as to enhance the original flow pattern. The results indicated that the overall performance of the mini-channel was enhanced effectively. The conclusions are drawn as follows:

(a) Flow patterns investigation. The main characteristic of the original flow pattern was the up-down counter flow in the transverse section. In the v-ribs roughened mini-channel, the multi-longitudinal swirls flow was generated, thereby maintaining the secondary flow intensity and enhancing the up-down counter flow intensity in the mini-channel.

(b) Thermal resistance and irreversibility analyses. In the v-ribs roughened mini-channel heat sink, the fluid thermal resistance was close in value to the solid thermal resistance. It indicated that the fluid thermal resistance was no longer the dominate impediment and that the heat transfer enhancement measure was effective. In addition, with specifying a constant heat flux, the irreversibility was decreased with the increase of convective heat transfer performance in this research range.

(c) Overall performance evaluations. The variation ranges of Nu/Nu_0, f/f_0, EEC, and R3 are 1.71–3.55, 2.76–7.99, 0.32–0.89, and 1.12–2.06, respectively, in the mini-channel. The configured parameters of $p_l/D_h = 1$ and $\alpha = 30°$ were recommended to achieve a larger R3 criterion in the mini-channel. The maximum average heat flux of the substrate can achieve 5.79 W/mm^2 within temperature difference of 60 K in the condition of $p_l/D_h = 1$, $\alpha = 45°$, and $Re = 6800$. The corresponding pressure gradient is 2520 Pa/mm.

Conflict of interests

There are no known conflicts of interest associated with this publication.

Declaration of Competing Interest

The authors declare that they have no known competing financial interests or personal relationships that could have appeared to influence the work reported in this paper.

CRediT authorship contribution statement

Hui Xiao: Conceptualization, Methodology, Validation, Formal analysis, Investigation, Data curation, Writing - original draft, Writing - review & editing. **Zhichun Liu:** Resources, Supervision, Project administration. **Wei Liu:** Resources, Supervision, Project administration, Funding acquisition.

Acknowledgement

This work was supported by the National Natural Science Foundation of China (Grant No. 51736004).

References

[1] N.H. Naqiuddin, L.H. Saw, M.C. Yew, F. Yusof, T.C. Ng, M.K. Yew, Overview of micro-channel design for high heat flux application, Renewable and Sustainable Energy Reviews 82 (2018) 901–914.
[2] D.B. Tuckerman, R.F.W. Pease, High-performance heat sinking for VLSI, IEEE Electron Device Letters 2 (5) (1981) 126–129.
[3] S. Kandlikar, S. Garimella, D. Li, S. Colin, M.R. King, Heat Transfer and Fluid Flow in Minichannels and Microchannels, 2nd ed., Elsevier, 2014.
[4] H. Xiao, Z. Dong, R. Long, K. Yang, F. Yuan, A Study on the Mechanism of Convective Heat Transfer Enhancement Based on Heat Convection Velocity Analysis, Energies 12 (21) (2019) 4175.
[5] H. Xiao, Z. Dong, Z. Liu, W. Liu, Heat transfer performance and flow characteristics of solar air heaters with inclined trapezoidal vortex generators, Appl Therm Eng 179 (2020) 115484.
[6] M. Sheikholeslami, M. Gorji-Bandpy, D.D. Ganji, Review of heat transfer enhancement methods: focus on passive methods using swirl flow devices, Renewable and Sustainable Energy Reviews 49 (2015) 444–469.
[7] J.J. Liu, Z.C. Liu, W. Liu, 3D numerical study on shell side heat transfer and flow characteristics of rod-baffle heat exchangers with spirally corrugated tubes, International Journal of Thermal Sciences 89 (2015) 34–42.
[8] Z. Sun, K. Zhang, W. Li, Q. Chen, N. Zheng, Investigations of the turbulent thermal-hydraulic performance in circular heat exchanger tubes with multiple rectangular winglet vortex generators, Appl Therm Eng 168 (2020) 114838.
[9] J. Liu, G. Xie, T.W. Simon, Turbulent flow and heat transfer enhancement in rectangular channels with novel cylindrical grooves, Int J Heat Mass Transf 81 (2015) 563–577.
[10] X.-w. Li, J.-a. Meng, Z.-y. Guo, Turbulent flow and heat transfer in discrete double inclined ribs tube, Int J Heat Mass Transf 52 (3) (2009) 962–970.
[11] T. Ma, Q.-w. Wang, M. Zeng, Y.-t. Chen, Y. Liu, V. Nagarajan, Study on heat transfer and pressure drop performances of ribbed channel in the high temperature heat exchanger, Appl Energy 99 (2012) 393–401.
[12] A.P. Singh, V. Siddhartha, Heat transfer and friction factor correlations for multiple arc shape roughness elements on the absorber plate used in solar air heaters, Experimental Thermal and Fluid Science 54 (2014) 117–126.
[13] P. Promvonge, S. Skullong, Heat transfer in solar receiver heat exchanger with combined punched-V-ribs and chamfer-V-grooves, Int J Heat Mass Transf 143 (2019) 118486.
[14] V. Kumar, Nusselt number and friction factor correlations of three sides concave dimple roughened solar air heater, Renew Energy 135 (2019) 355–377.
[15] M. Sheikholeslami, M. Jafaryar, M. Hedayat, A. Shafee, Z. Li, T.K. Nguyen, M. Bakouri, Heat transfer and turbulent simulation of nanomaterial due to compound turbulator including irreversibility analysis, Int J Heat Mass Transf 137 (2019) 1290–1300.
[16] P. Singh, M. Zhang, S. Ahmed, K.R. Ramakrishnan, S. Ekkad, Effect of micro-roughness shapes on jet impingement heat transfer and fin-effectiveness, Int J Heat Mass Transf 132 (2019) 80–95.
[17] B. Dai, M. Li, Y. Ma, Effect of surface roughness on liquid friction and transition characteristics in micro- and mini-channels, Appl Therm Eng 67 (1) (2014) 283–293.
[18] C. Bi, G.H. Tang, W.Q. Tao, Heat transfer enhancement in mini-channel heat sinks with dimples and cylindrical grooves, Appl Therm Eng 55 (1) (2013) 121–132.
[19] M. Attalla, H.M. Maghrabie, E. Specht, An experimental investigation on fluid flow and heat transfer of rough mini-channel with rectangular cross section, Experimental Thermal and Fluid Science 75 (2016) 199–210.
[20] K. Guo, B. Liu, X. Li, H. Liu, C. Liu, Flow pattern construction-based tubular heat transfer intensification using calculus of variations, Chem Eng Sci 152 (2016) 568–578.
[21] X. Chen, T. Zhao, M.-.Q. Zhang, Q. Chen, Entropy and entransy in convective heat transfer optimization: a review and perspective, Int J Heat Mass Transf 137 (2019) 1191–1220.
[22] W. Liu, P. Liu, J.B. Wang, N.B. Zheng, Z.C. Liu, Exergy destruction minimization: a principle to convective heat transfer enhancement, Int J Heat Mass Transf 122 (2018) 11–21.
[23] H. Xiao, J. Wang, Z. Liu, W. Liu, Turbulent heat transfer optimization for solar air heater with variation method based on exergy destruction minimization principle, Int J Heat Mass Transf 136 (2019) 1096–1105.
[24] Y.-.L. He, W.-.Q. Tao, Chapter Three - Convective Heat Transfer Enhancement: mechanisms, Techniques, and Performance Evaluation, in: E.M. Sparrow, Y.I. Cho, J.P. Abraham, J.M. Gorman (Eds.), Advances in Heat Transfer, Elsevier, 2014, pp. 87–186.
[25] W. Liu, P. Liu, Z.M. Dong, K. Yang, Z.C. Liu, A study on the multi-field synergy principle of convective heat and mass transfer enhancement, Int J Heat Mass Transf 134 (2019) 722–734.
[26] N. Zheng, F. Yan, K. Zhang, T. Zhou, Z. Sun, A review on single-phase convective heat transfer enhancement based on multi-longitudinal vortices in heat exchanger tubes, Appl Therm Eng 164 (2020) 114475.
[27] , IAPWS Industrial Formulation 1997 for the Thermodynamic Properties of Water and Steam, in: International Steam Tables: Properties of Water and Steam Based on the Industrial Formulation IAPWS-IF97, Berlin, Heidelberg, Springer Berlin Heidelberg, 2008, pp. 7–150.
[28] F.R. Menter, Review of the shear-stress transport turbulence model experience from an industrial perspective, Int J Comut Fluid Dyn 23 (4) (2009) 305–316.
[29] J. Liu, S. Hussain, J. Wang, L. Wang, G. Xie, B. Sundén, Heat transfer enhancement and turbulent flow in a high aspect ratio channel (4:1) with ribs of various truncation types and arrangements, International Journal of Thermal Sciences 123 (2018) 99–116.
[30] P.W. Deshmukh, S.V. Prabhu, R.P. Vedula, Heat transfer enhancement for laminar flow in tubes using curved delta wing vortex generator inserts, Appl Therm Eng 106 (2016) 1415–1426.
[31] H. Xiao, J. Wang, Z. Liu, W. Liu, A consistent SIMPLE algorithm with extra explicit prediction — SIMPLEPC, Int J Heat Mass Transf 120 (2018) 1255–1265.
[32] S.V. Patankar, Numerical HeatTransfer and Fluid Flow, Hemisphere, Washington D.C., 1980.
[33] L.M.F Moukalled, M. Darwish, The finite volume method in computational fluid dynamics, 2016.
[34] J. Holman, Heat Transfer, 10th ed., McGraw-Hill, Boston, MASS., 2010.
[35] A. Bejan, Entropy Generation Through Heat and Fluid Flow, Wiley, 1982.
[36] W. Liu, H. Jia, Z.C. Liu, H.S. Fang, K. Yang, The approach of minimum heat consumption and its applications in convective heat transfer optimization, Int J Heat Mass Transf 57 (1) (2013) 389–396.
[37] G. Lu, X. Zhai, Analysis on heat transfer and pressure drop of a microchannel heat sink with dimples and vortex generators, International Journal of Thermal Sciences 145 (2019) 105986.
[38] M.A. Alfellag, H.E. Ahmed, A.S. Kherbeet, Numerical simulation of hydrothermal performance of minichannel heat sink using inclined slotted plate-fins and triangular pins, Appl Therm Eng 164 (2020) 114509.